Article

Calculation of the Statistical Properties in Intermittency Using the Natural Invariant Density

Sergio Elaskar [1,*] , **Ezequiel del Río** [2] **and Denis Lorenzón** [3]

1 Departamento de Aeronáutica, Instituto de Estudios Avanzados en Ingeniería y Tecnología (IDIT), FCEFyN, Universidad Nacional de Córdoba and CONICET, Córdoba 5000, Argentina

2 Departamento de Física Aplicada, ETSIAE, Universidad Politécnica de Madrid, 28040 Madrid, Spain; ezequiel.delrio@upm.es

3 Instituto de Estudios Avanzados en Ingeniería y Tecnología (IDIT), Universidad Nacional de Córdoba and CONICET, Córdoba 5000, Argentina; denis.lorenzon@gmail.com

* Correspondence: selaskar@unc.edu.ar

Abstract: We use the natural invariant density of the map and the Perron–Frobenius operator to analytically evaluate the statistical properties for chaotic intermittency. This study can be understood as an improvement of the previous ones because it does not introduce assumptions about the reinjection probability density function in the laminar interval or the map density at pre-reinjection points. To validate the new theoretical equations, we study a symmetric map and a non-symmetric one. The cusp map has symmetry about $x = 0$, but the Manneville map has no symmetry. We carry out several comparisons between the theoretical equations here presented, the M function methodology, the classical theory of intermittency, and numerical data. The new theoretical equations show more accuracy than those calculated with other techniques.

Keywords: chaotic intermittency; maps; reinjection probability density function; invariant density

1. Introduction

In chaotic intermittency, the solutions of the dynamical systems exhibit the alternation between chaotic and laminar behaviors. The laminar phases, also called regular phases, are related to pseudo-equilibrium regions or pseudo-periodic solutions. The bursts correspond to chaotic behavior [1–4]. Intermittency has been observed in engineering, physics, medicine, chemistry, and economy [5–14]. In addition, intermittency has been associated with the symmetry breaking in chaotic and stochastic systems [15,16]. Therefore, a more complete and accurate description of the intermittency phenomenon would be applied in several subjects. In the classic theory, intermittency was classified into three types, I, II and III, and later, other types were introduced [17–23].

One-dimensional maps are widely used to study chaotic intermittency [1–4]. These maps have a mechanism to reinject the trajectories from the chaotic region to the laminar one, which determines the reinjection probability density (RPD) function [1,3]. The RPD function describes the probability of the trajectories to be reinjected at each point of the laminar interval. Usually, once the RPD is calculated, other statistical functions can be obtained as the probability density of the laminar lengths (PDLLs), the characteristic relation, etc. The reinjection process can be very complex as indicated in [24]. Accordingly, an accurate calculation of the RPD function and other statistical properties is essential to explain the intermittency phenomenon.

We note that there was not a general methodology to obtain the RPD, and distinct schemes were utilized. The classical theory of intermittency considers a uniform RPD function. This assumption generates the classic characteristic relations, which establish how the average laminar length tends to infinity as a control parameter tends to zero [1,2,25]. A more general RPD has been introduced in the last few years. Accordingly, the characteristic relations were generalized too. To calculate this general RPD, the M function

methodology was developed, which has worked accurately for maps with types I, II, III and V intermittencies without and with noise. The M function methodology uses a less restrictive assumption of a constant density at points that govern the reinjection process, i.e., pre-reinjection points [3,26–35].

In this paper, we introduce a new methodology to evaluate the RPD function, $\phi(x)$, and other statistical properties. We call it the density technique. To develop this technique, we use the Perron–Frobenius operator and the invariant density of the map. This study does not introduce assumptions about the RPD in the laminar interval, as does the classical theory, or the map density at pre-reinjection points, as does the M function methodology, because it uses the invariant density of the map. To validate the new theoretical equations, we analyze the cusp map [36,37] and the classical Manneville map [4,38]. The cusp map is symmetric about the axis $x = 0$, and the Manneville map has no geometric symmetry. Therefore, we study the new methodology in symmetric and non-symmetric maps. We carry out several comparisons between the theoretical results here presented, the classical theory of intermittency, the M function methodology, and numerical data.

2. The Perron–Frobenius Operator

The Perron–Frobenius operator is used here to transform random variables. Therefore, we briefly describe this operator. A more complete explanation about the Perron–Frobenius operator can be found in [37,39].

Let us study a family of evolution operators $F^t(x) : \mathbb{D} \to \mathbb{D}$, such as $F^0 = $ identity and $F^{t_1+t_2} = F^{t_1} \circ F^{t_2}$, where $\mathbb{D}$ is a compact manifold, $x \in \mathbb{D}$, and t is the evolution variable. If t takes only discrete values, the operator $F^t(x)$ is a map. There are, at least, two formulations to describe the behavior of $F^t(x)$. One formulation corresponds to study the evolution of individual trajectories, the other one considers the evolution of the trajectories' density.

For $F^t(x) : \mathbb{R} \to \mathbb{R}$, the Perron–Frobenius operator evaluates the evolution of the trajectories' density. We analyze a map $y = F(x)$, which transforms some interval $\Delta_0 \subset \mathbb{R}$ in another interval $\Delta \subset \mathbb{R}$. Then, $x \in \Delta_0$ and $y \in \Delta$. In Δ_0, the density of trajectories is $\rho_0(x)$, while in Δ the trajectories' density is $\rho(y)$. The Perron–Frobenius operator, $\mathcal{L}$, evaluates the density ρ from ρ_0, and we write $\rho = \mathcal{L} \circ \rho_0$. If $\Delta = [a, y]$, where y is variable, the Perron–Frobenius operator calculates the density $\rho(y)$

$$\rho(y) = \frac{d}{dy} \int_{F^{-1}[a,y]} \rho_0(x) \, dx = \rho_0(F^{-1}(y)) \left| \frac{dF^{-1}(y)}{dy} \right|. \tag{1}$$

Note that Equation (1) supposes that $F(x)$ is differentiable and invertible with continuous $\frac{d \, F^{-1}(x)}{d \, x}$ [39]. On the other hand, the theoretical formulation of the M function methodology requires that $\frac{d \, F(x)}{d \, x}$ exists [3,30].

Let us now introduce a map $y = F(x)$, which is piecewise differentiable and satisfies $|F'(x)| \neq 0$, except in a finite number of critical points. Suppose that Δ is an interval containing no critical values, and suppose that $F^{-1}(\Delta)$ is the union of finitely many intervals, I_j, each of which is mapped monotonically onto Δ, then the Perron-Frobenius operator allows us to evaluate the density evolution:

$$\rho(y) = \sum_{y=F(x)|_{I_j}} \left. \frac{\rho_0(x)}{\left| \frac{dF(x)}{dx} \right|} \right|_{I_j}, \quad \text{with} \quad j = 1, ..., z \tag{2}$$

where z is the number of intervals.

3. Evaluation of Statistical Properties

In this section, we calculate several functions and parameters to describe chaotic intermittency. First, we study the RPD function, then we analyze other statistical properties: the PDLL function, the characteristic relation, the intermittency factor, the number of

iterations in the laminar and non-laminar phases, and the number of times that a trajectory crosses the boundary between laminar and non-laminar zones.

3.1. Evaluation of the RPD

The probability measure in an interval S can be written as

$$P(S) = \lim_{N \to \infty} \frac{1}{N} \sum_{n=0}^{N} J_S(x_n), \tag{3}$$

where $J_S(x)$ is the characteristic function of the interval S

$$J_S(x) = \begin{cases} 1, & \text{if} \quad x \in S \\ 0, & \text{if} \quad x \notin S. \end{cases} \tag{4}$$

Therefore, the probability measure shows the frequency that the trajectory reaches the interval. We can relate the invariant density, $\rho(x)$, with the probability measure, $P(S)$, by

$$P(S) = \int_S \rho(x)dx. \tag{5}$$

Now, we divide the whole data series into three subsets

$$\{x_n\} = \{x_{n'}\} \cup \{x_{n''}\} \cup \{x_{n'''}\}. \tag{6}$$

First, we select $x_{n'+1} \in S$ and in the preceding iteration it has already been there, that is $J_S(x_{n'+1}) = 1$ and $J_S(x_{n'}) = 1$. For the next one, we have $x_{n''+1} \in S$ but in the preceding period it has not been there, that is $J_S(x_{n''+1}) = 1$ and $J_S(x_{n''}) = 0$. Finally, $x_{n'''} \notin S$. Note that there is no intersection between them.

$$\{x_{n'}\} \cap \{x_{n''}\} = \{x_{n''}\} \cap \{x_{n'''}\} = \{x_{n'''}\} \cap \{x_{n'}\} = \varnothing. \tag{7}$$

Therefore, the probability measure $P(S)$ can be written as

$$P(S) = \lim_{N \to \infty} \frac{1}{N} \sum_{n'=0}^{N} J_S(x_{n'}) + \lim_{N \to \infty} \frac{1}{N} \sum_{n''=0}^{N} J_S(x_{n''}). \tag{8}$$

The first term in the RHS is the probability for the trajectory to be in S when in the previous iteration it has been there. If $S = I_L$ (where I_L is the laminar interval), then, only the second term in the RHS determines the RPD function, $\phi(x)$, through the relation

$$\lim_{N \to \infty} \frac{1}{N} \sum_{n=0}^{N} J_{I_L}(x_{n''}) = w \int_{I_L} \phi(x)dx. \tag{9}$$

The weight w is included because it is current to normalize the RPD function over the laminar interval I_L as $\int_{I_L} \phi(x)dx = 1$. Therefore, to obtain the RPD function, the sum in Equation (2) must exclude the contributions that do not generate reinjection in the laminar zone [3,40]

$$\phi(x) = w \sum_{j \neq l}^{n} \left| \frac{dF_j^{-1}(x)}{dx} \right| \rho(F_j^{-1}(x)), \tag{10}$$

where l indicates the intervals that do not generate reinjection and $\rho(F_j^{-1}(x))$ is the density in the preceding iteration to reinjection. The weight w can be calculated from the normalization condition:

$$\int_{I_L} \phi(x)\,dx = \sum_{j \neq l}^{n} \int_{I_L^{-1}} \rho(F_j^{-1}(x))\,dx = 1. \tag{11}$$

We can organize the intervals I_j following

$$
\begin{cases}
x_{n'-1} \in I_j, & \text{with} \quad j = 1, ... h \\
x_{n''-1} \in I_k, & \text{with} \quad k = h+1, ... z.
\end{cases}
\tag{12}
$$

Therefore, Equation (2) can be written as

$$
\rho(y) = \sum_{y=F(x)|_{I_j}} \frac{\rho_0(x)}{\left|\frac{dF(x)}{dx}\right|}\Bigg|_{I_j} + \sum_{y=F(x)|_{I_k}} \frac{\rho_0(x)}{\left|\frac{dF(x)}{dx}\right|}\Bigg|_{I_k}
\tag{13}
$$
$$
\text{with} \quad j = 1, ..., h, \quad \text{and} \quad k = h+1, ..., z.
$$

If the map $F(x)$ has an invariant density, ρ, it verifies $\rho = L \circ \rho$. Then, Equation (13) becomes

$$
\rho(y) = \sum_{y=F(x)|_{I_j}} \frac{\rho(x)}{\left|\frac{dF(x)}{dx}\right|}\Bigg|_{I_j} + \sum_{y=F(x)|_{I_k}} \frac{\rho(x)}{\left|\frac{dF(x)}{dx}\right|}\Bigg|_{I_k}
\tag{14}
$$
$$
\text{with} \quad j = 1, ..., h, \quad \text{and} \quad k = h+1, ..., z.
$$

Using Equations (10) and (14), the RPD function can be calculated by two alternative equations. The first one is

$$
\phi(y) = w \sum_{y=F(x)|_{I_k}} \frac{\rho(x)}{\left|\frac{dF(x)}{dx}\right|}\Bigg|_{I_k} \quad \text{with} \quad k = h+1, ..., z,
\tag{15}
$$

and the second one results

$$
\phi(y) = w \left(\rho(y) - \sum_{y=F(x)|_{I_j}} \frac{\rho(x)}{\left|\frac{dF(x)}{dx}\right|}\Bigg|_{I_j} \right) \quad \text{with} \quad j = 1, ..., h.
\tag{16}
$$

Equation (15) calculates the RPD from points outside the laminar interval that are reinjected inside it, i.e., points $x_{n''}$ that verify $J_S(x_{n''+1}) = 1$ and $J_S(x_{n''}) = 0$. In contrast, Equation (16) evaluates the RPD function by subtracting from the invariant density points that were in the laminar interval at the previous iteration and that remain in it, i.e., points $x_{n'}$ that verify $J_S(x_{n'+1}) = 1$ and $J_S(x_{n'}) = 1$. Finally, the RPD function must satisfy the normalization condition given by Equation (11).

We emphasize that Equations (15) and (16) establish new analytical relationships between the invariant density, ρ, and the RPD function, ϕ, for chaotic intermittency.

3.2. Evaluation of Other Statistical Properties

For each reinjected point x, there is a laminar length $l(x)$, which determines the number of iterations that the trajectory needs to move from x to the boundary of the laminar interval c. Thus, the PDLL function establishes the probability of finding laminar intervals of length l. Usually, the PDLL function is obtained from the RPD function as follows [1,3]

$$
\psi(l, c) = \phi(y(l)) \left| \frac{dy(l)}{dl} \right|.
\tag{17}
$$

Here, we evaluate the PDLL function using the invariant density of the map without calculating previously the RPD function. If we introduce Equation (15) in Equation (17), we obtain

$$
\psi(l, c) = w \sum_{y=F(x)|_{I_k}} \rho(x(l)) \left| \frac{dx(l)}{dl} \right|\Bigg|_{I_k} \quad \text{with} \quad k = h+1, ..., z,
\tag{18}
$$

where x represents the pre-reinjection points, $y = F(x)$ and $y \in I_L$. From the last equation, we calculate the probability density of the laminar lengths directly from the invariant density of the map.

In addition, the characteristic relation, $L = L(\varepsilon)$, can be calculated from the invariant density

$$L = \int_{l \in I_L} \psi(l,c)\, l \, dl = w \int_{F^{-1}(I_L)} \sum_{y = F(x)|_{I_k}} l(x)\, \rho(x) \Bigg|_{I_k} dx \quad \text{with} \quad k = h+1, ..., z, \quad (19)$$

where L is the average laminar length.

Directly from the invariant density, we can determine the "time" that the trajectory spends in laminar and non-laminar behaviors. Let us consider a process with $N_t = N_l + N_c$ iterations. Where N_l and N_c are the numbers of iterations inside and outside of the laminar interval, respectively,

$$N_l = \int_{I_L} \rho(x)\, dx, \quad N_c = \int_{I_C} \rho(x)\, dx, \quad (20)$$

$I_T = I_L \cup I_C$ is the interval where the map is defined, and there is no intersection between I_L and I_C: $I_L \cap I_C = \emptyset$. The relation between them is

$$\sigma = \frac{\int_{I_L} \rho(x)\, dx}{\int_{I_C} \rho(x)\, dx}. \quad (21)$$

Note that $\sigma = \sigma(\varepsilon)$, where ε is the parameter controlling the route from regular to chaotic behavior.

From the previous relation, we can obtain the average non-laminar length, C

$$C = \frac{L}{\sigma}, \quad (22)$$

where the average laminar length, L, is given by Equation (19).

The intermittency factor, γ, determines the probability that a trajectory is outside the laminar interval. It can be calculated from the invariant density as

$$\gamma = \frac{\int_{I_C} \rho(x)\, dx}{\int_{I_T} \rho(x)\, dx} = \int_{I_C} \rho(x)\, dx. \quad (23)$$

Finally, the number of times a trajectory crosses the boundary between the laminar and non-laminar interval results

$$N_{lc} = \frac{N_t}{L \left(\frac{1}{\sigma} + 1 \right)}. \quad (24)$$

Note that γ and N_{lc} also depend on ε.

For a map with intermittency, Equations (18)–(24) allow us to directly calculate the probability density of the laminar lengths, the average laminar and non-laminar lengths, the characteristic relation, the number of iterations in laminar and non-laminar phases, the intermittency factor, and the number of crosses between the laminar and non-laminar zones without the evaluation of the reinjection probability density function.

4. Application to the Cusp Map

Let us introduce the following map:

$$F(x) = 1 + \varepsilon - 2\sqrt{|x|}. \quad (25)$$

Note that for $\varepsilon = 0$, the cusp map is recovering [36,37]. For $\varepsilon = 0$, the map has a fixed point at $x_0 = -1$, which disappears for $\varepsilon > 0$, and for $0 < \varepsilon \ll 1$ type-I intermittency occurs. Figure 1 shows the map given by Equation (25) for $\varepsilon = 0.0001$. Note that the cusp map given by Equation (25) has symmetry about $x = 0$.
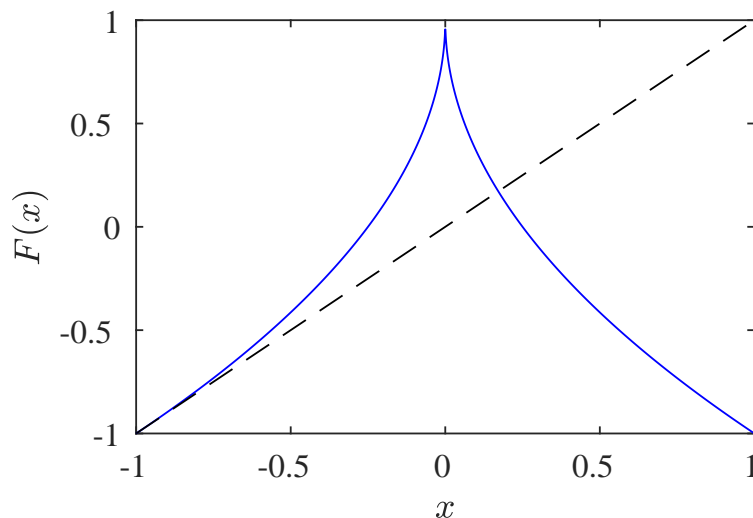

Figure 1. Cusp map for $\varepsilon = 0.0001$.

The cusp map has an invariant density $\rho(x)$ [37]

$$\rho(x) = \frac{1 - x}{2}. \tag{26}$$

For the map (25), the number of intervals is $z = 2$, and $j = 1$, $k = 2$. In accordance with Equation (15), the RPD function results

$$\phi(y) = w \left. \frac{\rho(x)}{\left| \frac{dF(x)}{dx} \right|} \right|_{I_2}, \tag{27}$$

and using Equation (16), the RPD function can be calculated as

$$\phi(y) = w \left(\rho(y) - \left. \frac{\rho(x)}{\left| \frac{dF(x)}{dx} \right|} \right|_{I_1} \right), \tag{28}$$

if $y = 1 - 2\sqrt{|x|}$, I_1 is defined as

$$x_1 = F_1^{-1}(y) = -\left(\frac{1 - y}{2} \right)^2, \quad x_1 \in I_1 = [-1, 0), \tag{29}$$

and I_2

$$x_2 = F_2^{-1}(y) = \left(\frac{1 - y}{2} \right)^2, \quad x_2 \in I_2 = (0, 1]. \tag{30}$$

The derivative $|d\,F(x)/dx|_{x_1, x_2}$ is

$$\left| \frac{d\,F(x)}{dx} \right|_{x_1, x_2} = \frac{2}{1 - x}. \tag{31}$$

Then, from Equations (26), (27) or (28) and (31), the RPD can be obtained

$$\phi(x) = w \left(\frac{1-x}{2} \left(\frac{1}{2} - \frac{(1-x)^2}{8} \right) \right),$$ (32)

where w is calculated from the normalization condition, Equation (11)

$$\int_{F_2^{-1}(x_0)}^{F_2^{-1}(x_0+c)} \rho(F_2^{-1}(x)) \, dx = \int_{x_0}^{x_0+c} \phi(x) \, dx = 1,$$ (33)

x_0 is the fixed point, and c is the semi-amplitude of the laminar interval, $I_L = [x_0, x_0 + c]$.

Results

To validate the previous theoretical equations, we perform the comparison between the RPD function given by Equation (32) with those calculated by the M function methodology, the classical theory, and with numerical data. A detailed explanation of the M function methodology can be found in Refs. [3,29–35]. The RPD calculated using the M function methodology results

$$\phi(x) = \frac{\alpha + 1}{c^{\alpha+1}} (x - x_0)^\alpha.$$ (34)

To evaluate the Equation (34), we use the function $M(x)$ defined as

$$M(x) = \begin{cases} \frac{\int_{x_s}^x \tau \, \phi(\tau) \, d\tau}{\int_{x_s}^x \phi(\tau) \, d\tau} & \text{if } \int_{x_s}^x \phi(\tau) d\tau \neq 0 \\ 0 & \text{if } \int_{x_s}^x \phi(\tau) d\tau = 0, \end{cases}$$ (35)

where $x_s < x$ for all reinjected points x. Note that the function $M(x)$ can be calculated as the average of reinjection points in the interval $[x_s, x]$, then, if we arrange the reinjections following the relation $x_j < x_{j+1}$, a very simple evaluation of the function $M(x)$ can be obtained

$$M(x_r) \approx \frac{\sum_{j=1}^r x_j}{r}.$$ (36)

We emphasize that Equation (36) does not need to know the function $\phi(x)$. For the RPD given by Equation (34), $M(x)$ is a linear function

$$M(x) = m \, (x - x_0) \quad x > x_0$$ (37)

where α in Equation (34) is obtained from the slope m

$$\alpha = \frac{2m - 1}{1 - m}.$$ (38)

On the other hand, the classical theory of intermittency assumes uniform reinjection, $\phi(x) = $ constant. Note that the classical theory is only a particular case of Equation (34) for $\alpha = 0$ ($m = 1/2$).

We emphasize that, to obtain Equation (34), the assumption of constant density at pre-reinjection points was introduced (see [3,30]).

To calculate the numerical data, we generate an iterative process for the map given by Equation (25); also, we divide the laminar interval into N_s sub-intervals, then we calculate the histogram of reinjections and the numerical RPD function. To obtain the histogram, we consider at least $50 \, N_s$ reinjections, which implies millions of iterations.

We develop several numerical tests for a different number of reinjected points N, and we split the laminar interval into N_s sub-intervals where the RPD functions are evaluated. To study the convergence process of the theoretical RPD functions given by

Equations (32) and (34) and the classical theory of intermittency regarding the numerical data, we evaluate

$$E_r = \frac{\sum_{j=1}^{j=N_s} \frac{|\phi_t(j) - \phi_n(j)|}{\phi_t(j)}}{N_s}, \qquad D_r = \sqrt{\frac{\sum_{j=1}^{j=N_s} \frac{(\phi_t(j) - \phi_n(j))^2}{(\phi_t(j))^2}}{N_s^2}}, \tag{39}$$

where $\phi_t(j)$ and $\phi_n(j)$ are the theoretical and numerical values of the RPD in the sub-interval j.

We study two sets of tests. For the first one, we consider the following parameters $N_s = 500$, $\varepsilon = 0.0001$, and $c = 0.2$. Figure 2a,b show $\ln(D_r)$ and $\ln(E_r)$ respectively, for different numbers of reinjected points, N from 100,000 to 2,500,000. We emphasize that as the number of reinjected points increases, the accuracy of the density technique and the M function methodology increases too. In addition, we note that the errors generated by Equation (32) are lower than those obtained from Equation (34). On the other hand, the M function methodology obtains $\alpha \approx 0.9056$. Theoretical and numerical RPDs are shown in Figure 3, the black points are the numerical data, the blue, green, and red lines are the RPD functions given by Equations (32) and (34) and the classical theory, respectively. From Figures 2a,b and 3, we can observe the convergence and accuracy of the theoretical formulation here presented.
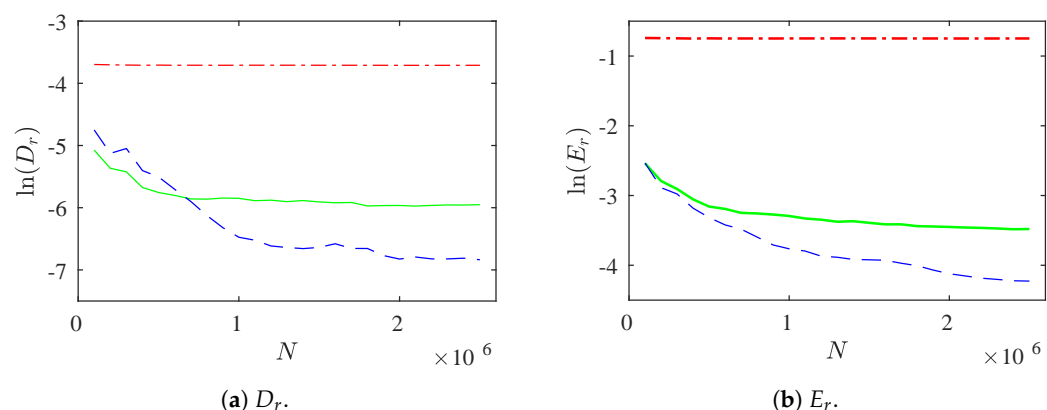

(a) D_r.   **(b)** E_r.

Figure 2. $\ln(D_r)$ and $\ln(E_r)$ vs. N for $\varepsilon = 0.0001$, $c = 0.2$, and $N_s = 500$. Blue line: density technique. Green line: M function methodology. Red line: classical theory.
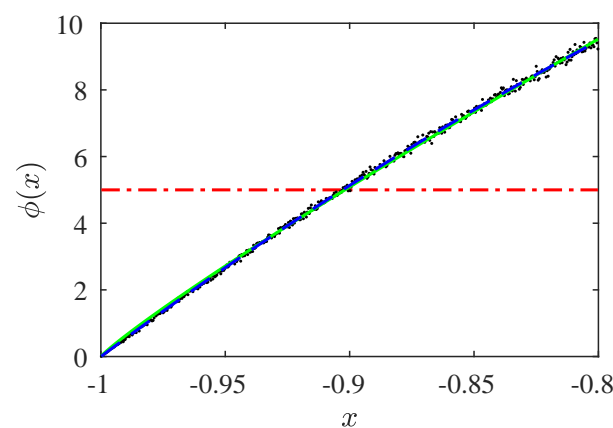

Figure 3. RPD function for $\varepsilon = 0.0001$, $c = 0.2$, $N_s = 500$, and $N = 2,500,000$. Blue line: density technique. Green line: M function methodology. Red line: classical theory. Black points: numerical data.

To calculate the rate of convergence of the results, we utilize the sequence $\{\frac{1}{N^p}\}_{N=1}^{\infty}$ that tends to zero when N tends to infinite, and we must verify

$$|D_r| \leq K_d \frac{1}{N^{p_d}}, \qquad |E_r| \leq K_e \frac{1}{N^{p_e}}, \qquad (40)$$

where K_d, K_e, p_d and p_e are positive real numbers. Then, we can say that $\{D_r\}_{N=1}^{\infty}$ and $\{E_r\}_{N=1}^{\infty}$ converge to zero with rate, or order, of convergence $O(\frac{1}{N^{p_d}})$ and $O(\frac{1}{N^{p_e}})$, respectively [41]. For this test, we find that $p_d \approx 0.45$ and $p_e \approx 0.5$. Therefore, D_r and E_r converge to zero when N tends to infinity.

The second set of tests uses the following parameters $N_s = 500$, $\varepsilon = 0.001$, and $c = 0.5$. Figure 4a,b show $\ln(D_r)$ and $\ln(E_r)$, respectively, for $N = 100{,}000$–$2{,}500{,}000$. Similar to the previous tests, as the number of reinjected points increases the accuracy of RPD calculated by the M function and the new theoretical formulation increases too. Again, the classical theory has the worst behavior. Additionally, we note that the errors generated by Equation (32) are lower than those obtained from Equation (34). As in the previous set of tests, the M function methodology obtains $\alpha \approx 0.9056$. Theoretical and numerical RPDs are shown in Figure 5, the black points are the numerical data, the blue, green, and red lines are the RPD functions given by Equations (32) and (34) and the classical theory, respectively.
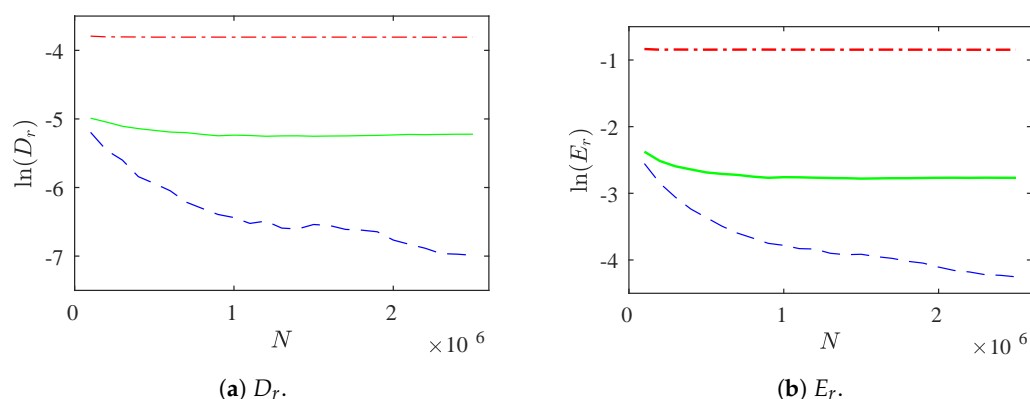

(a) D_r.   (b) E_r.

Figure 4. $\ln(D_r)$ and $\ln(E_r)$ vs. N for $\varepsilon = 0.001$, $c = 0.5$, and $N_s = 500$. Blue line: density technique. Green line: M function methodology. Red line: classical theory.
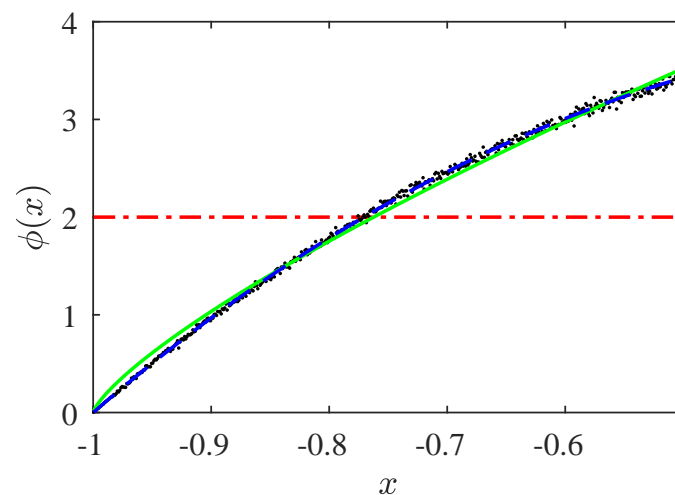

Figure 5. RPD function for $\varepsilon = 0.001$, $c = 0.5$, $N_s = 500$, and $N = 2{,}500{,}000$. Blue line: density technique. Green line: M function methodology. Red line: classical theory. Black points: numerical data.

If we apply Equation (40) for the density technique, we obtain $p_d \approx p_e \approx 0.5$, then D_r and E_r converge to zero for $N \to \infty$.

5. Application to the Manneville Map

The following map

$$F(x) = (1 + \varepsilon)\,x + (1 - \varepsilon)\,x^2 \pmod 1 \tag{41}$$

is the classical map introduced by Manneville [4]. For this map, $x_0 = 0$ is a stable fixed point for $-2 < \varepsilon < 0$, and for $0 < \varepsilon \ll 1$, the point loses its stability and type II intermittency occurs. The map is shown in Figure 6 for $\varepsilon = 0.001$. We highlight that the Manneville map given by Equation (41) has no geometric symmetry.
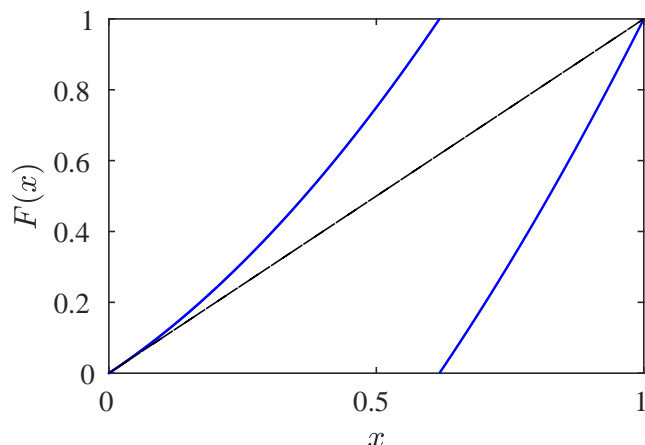

Figure 6. Manneville map for $\varepsilon = 0.001$.

The invariant density for this map was deduced in [42]

$$\rho(x) = K\left(\frac{1}{\varepsilon + (1 - \varepsilon)\,x} + \frac{1}{1 + (1 - \varepsilon)\,x}\right), \quad x \in [0, 1), \tag{42}$$

we have introduced K to normalize the density inside the interval $[0, 1)$

$$\int_0^1 \rho(x)\,dx = 1 \;\Rightarrow\; K = \frac{1 - \varepsilon}{\ln(2 - \varepsilon) - \ln(\varepsilon)}. \tag{43}$$

The number of intervals is $z = 2$, with $j = 1$, and $k = 2$. From Equation (15), the RPD function can be obtained as:

$$\phi(y) = w\,\frac{\rho(x_2)}{\left|\frac{dF(x)}{dx}\right|}\Bigg|_{I_2}. \tag{44}$$

The points x_2 inside the interval I_2 are

$$x_2(y) = F_2^{-1}(y) = \frac{1 + \varepsilon - (5 + \varepsilon^2 + 4y - 2\varepsilon(1 + 2y))^{0.5}}{2(\varepsilon - 1)}, \tag{45}$$

where $x_2 \in I_2 = [x_m, 1)$ and $y = F_2(x) = (1 + \varepsilon)\,x + (1 - \varepsilon)\,x^2 - 1$.

The density $\rho(x_2)$ is written in function of y as

$$\rho(x_2(y)) = \frac{(-1 + \varepsilon)\sqrt{5 + \varepsilon^2 + 4y - 2\varepsilon(1 + 2y)}}{(-1 + (-1 + \varepsilon)y)(\ln(2 - \varepsilon) - \ln(\varepsilon))}, \tag{46}$$

and

$$\left|\frac{dF(x)}{dx}\right|_{x_2} = \sqrt{|5 + \varepsilon^2 + 4y - 2\varepsilon(1 + 2y)|}. \tag{47}$$

From these last equations and the normalization condition, we obtain

$$\phi(y) = \frac{(1-\varepsilon)}{((1-\varepsilon)y + 1)\ln(1 + c(1-\varepsilon))} . \tag{48}$$

Results

We present some numerical and theoretical results for the Manneville map (Equation (41)). We study two sets of tests with different parameters. The first set uses $\varepsilon = 0.001$, $c = 0.1$, $N = 100{,}000$–$2{,}500{,}000$ and $N_s = 500$. The results are shown in Figures 7a,b and 8. Figure 7a,b show the evolution of $\ln(D_r)$ and $\ln(E_r)$ vs. N. The results evaluated by the density technique are the dashed blue line, the green line corresponds to the M function methodology, and the red line to the classical theory. From these figures, we observe that the density technique approximates more accurately the RPD than the M function methodology and the classical theory. Figure 8 shows the RPD functions, the blue line is the RPD calculated by the density technique (Equation (48)), the green line is the RPD obtained by M function methodology (Equation (34)), the red line represents the classical RPD, and the black points are the numerical data. We note that the theoretical RPD calculated by Equation (48) captures accurately the numerical data. In addition, we emphasize that the RPD is approximately constant.

To evaluate the rate of convergence of these results, we use the Equation (40). For this set of tests, we obtain $p_d \approx 0.45$ and $p_e \approx 0.4$. Then, D_r and E_r converge to zero when N tends to infinity with a rate of convergence $O(\frac{1}{N^{0.45}})$ and $O(\frac{1}{N^{0.4}})$, respectively.

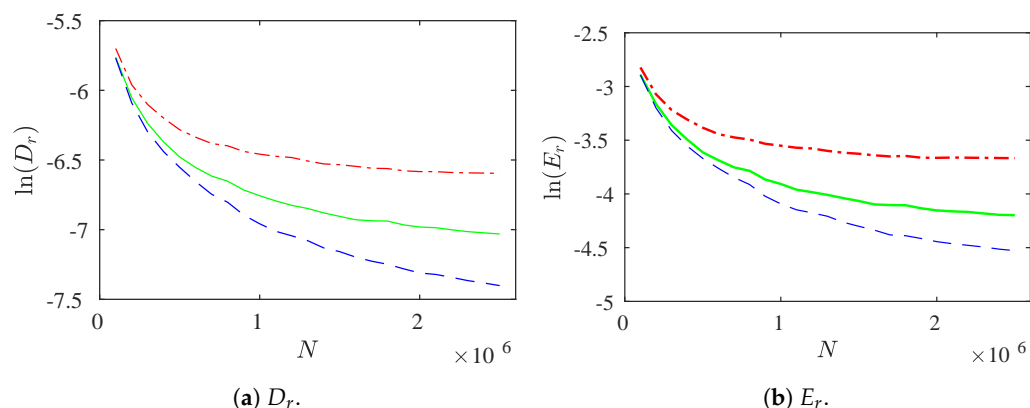(**a**) D_r.   (**b**) E_r.

Figure 7. Manneville map. $\ln(D_r)$ and $\ln(E_r)$ vs. N for $\varepsilon = 0.001$, $c = 0.1$, and $N_s = 500$. Blue line: density technique. Green line: M function methodology. Red line: classical theory.
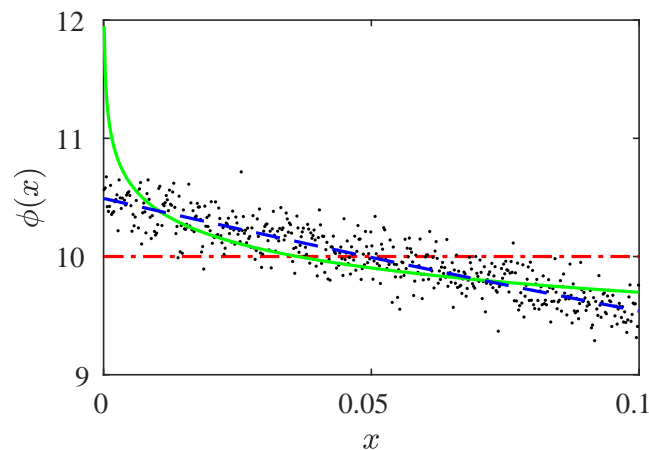

Figure 8. Manneville map. RPD functions for $\varepsilon = 0.001$, $c = 0.1$, $N_s = 500$, and $N = 2{,}500{,}000$. Blue line: density technique. Green line: M function methodology. Red line: classical theory. Black points: numerical data.

For this test, with $N_t = 500{,}000{,}000$, we also calculate N_l, N_c, σ, C, γ, and N_{lc}. The comparison between numerical and theoretical results is shown in Table 1. The first file has the theoretical values calculated using Equations (18)–(24), the second file shows the numerical data, and the third one contains the percentage error

$$E = \frac{V_t - V_n}{V_n}\, 100\,. \tag{49}$$

where V_t and V_n are the theoretical and numerical values, respectively.

Table 1. Test 1: $\varepsilon = 0.001$ and $c = 0.1$. Comparison between numerical and theoretical values for N_l, N_c, σ, L, C, γ, and N_{lc}.

	N_l	N_c	σ	L	C	γ	N_{lc}
Theoretical	0.620	0.380	1.629	47.97	29.448	0.380	6,458,394
Numerical	0.622	0.378	1.645	49.23	29.076	0.378	6,218,278
Error (E)	-0.32%	0.529%	-0.97%	-2.55%	1.278%	0.529%	3.86%

From Table 1, good accuracy can be observed between theoretical results and numerical data.

Using Equation (19), we calculate the characteristic relation for $c = 0.1$. Figure 9 shows the numerical (red points) and theoretical (blue points) results. Note that the characteristic relation can be written as

$$L = l_0 + A\ln(\varepsilon)\,, \tag{50}$$

The dashed red and blue lines are the linear interpolation for the numerical and theoretical data with $A = -10.24$ and $A = -10.38$, respectively. Note that $A \cong -1/c$. Therefore, the characteristic relation verifies $L \propto \ln(\varepsilon)$.
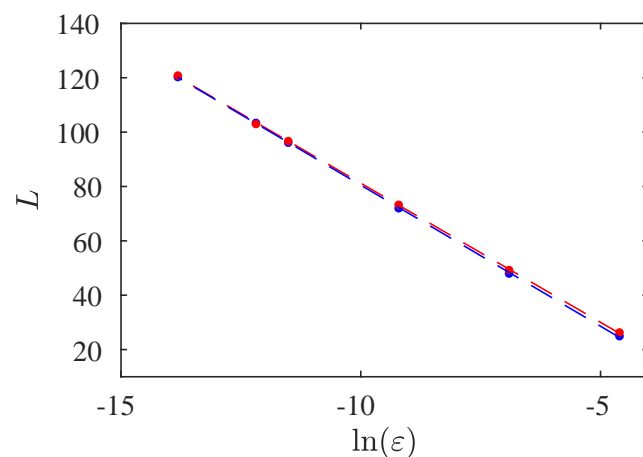

Figure 9. Manneville map. Characteristic relation for $c = 0.1$. Blue points: density technique. Red points: numerical data. Blue dashed line: linear interpolation for theoretical data, $A = -10.38$. Red dashed line: linear interpolation for numerical data, $A = -10.24$.

Note that for $c \ll 1$, Equation (48) can be approximated in the laminar interval $[0, c)$ by a constant function

$$\phi(x) \approx 1/c\,. \tag{51}$$

For an RPD that satisfies the last equation, the characteristic relation is given by Equation (50) with $A = -1/c$ (see Ref. [38]).

For the second set, we use the following parameters, $\varepsilon = 0.0001$, $c = 0.05$, $N = 100{,}000$–$2{,}500{,}000$ and $N_s = 350$. Figures 10a,b and 11 show the results. The evolution of $\ln(D_r)$ and $\ln(E_r)$ for different N is shown in Figure 10a,b. The blue, green, and red lines correspond to the density technique, the M function methodology, and the classical theory, respectively. The best results are obtained for the density technique. Figure 11 shows the RPD functions, the blue, green and, red lines are the RPDs calculated by the density technique (Equation (48)), the M function methodology (Equation (34)), and the classical theory, respectively, the black points are the numerical data. The theoretical RPD calculated by density technique captures accurately the numerical data.

The rate of convergence of these results is evaluated by Equation (40). We obtain $p_d \approx p_e \approx 0.45$. Accordingly, D_r, $E_r \to 0$ for $N \to \infty$ with a rate of convergence $O(\frac{1}{N^{0.45}})$.
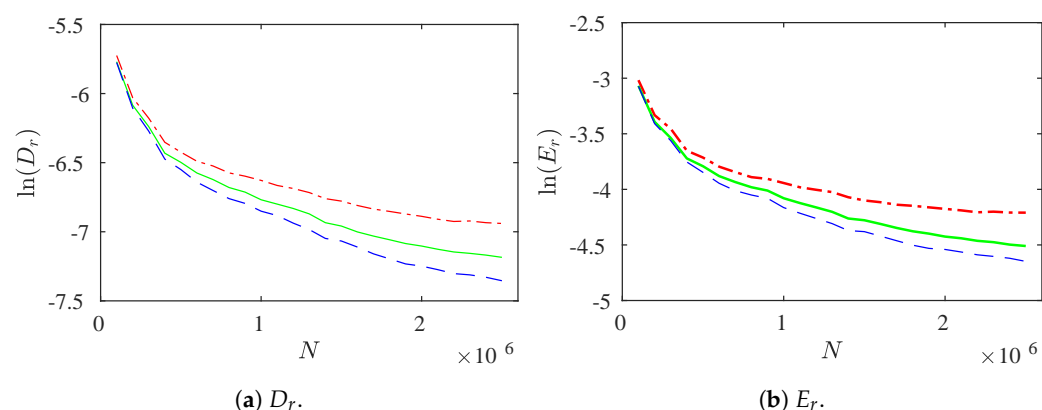

(**a**) D_r. (**b**) E_r.

Figure 10. Manneville map. $\ln(D_r)$ and $\ln(E_r)$ vs. N for $\varepsilon = 0.0001$, $c = 0.05$, and $N_s = 350$. Blue line: density technique. Green line: M function methodology. Red line: classical theory.
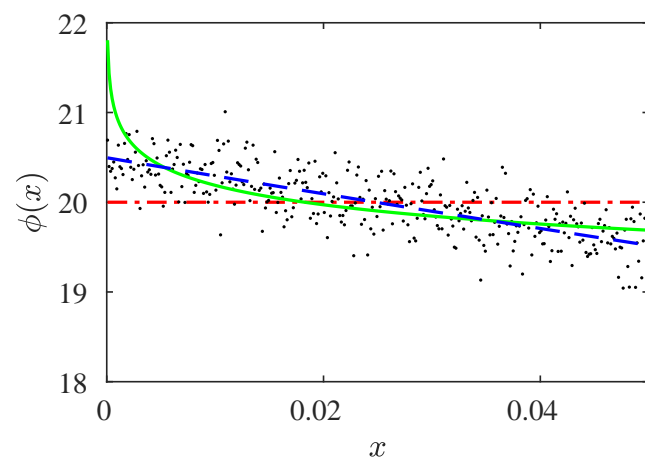

Figure 11. Manneville map. RPD functions for $\varepsilon = 0.0001$, $c = 0.05$, $N_s = 350$, and $N = 2{,}500{,}000$. Blue line: density technique. Green line: M function methodology. Red line: classical theory. Black points: numerical data.

We observe that the better results are calculated using the density technique here introduced.

In addition, we calculate with $N_t = 500{,}000{,}000$ the following variables: N_l, N_c, σ, C, γ, and N_{lc}. The comparison between numerical and theoretical results is shown in Table 2. The first, second, and third files show the theoretical values calculated using Equations (18)–(24), the numerical data, and the percentage error given by Equation (49), respectively.

Table 2. Test 2: $\varepsilon = 0.0001$ and $c = 0.05$. Comparison between numerical and theoretical values for N_l, N_c, σ, L, C, γ, and N_{lc}.

	N_l	N_c	σ	L	C	γ	N_{lc}
Theoretical	0.6326	0.3674	1.722	126.89	73.68	0.3674	2,492,860
Numerical	0.632	0.368	1.717	128.16	74.64	0.368	2,468,143
Error (E)	0.095%	−0.16%	0.29%	−0.99%	−1.28%	−0.16%	1%

From Table 2, high accuracy can be observed between calculated numerical and theoretical results.

We evaluate, using Equation (19), the characteristic relation for $c = 0.05$. Figure 12 shows the numerical (red points) and theoretical (blue points) results. The red and blue dashed lines are the linear interpolations of the numerical and theoretical data, respectively. The characteristic relation calculated by the numerical data can be approximated by (red dashed line)

$$L = -19.99 \ln(\varepsilon) - 55.43 \tag{52}$$

and the characteristic relation evaluated using theoretical results is (blue dashed line)

$$L = -20.14 \ln(\varepsilon) - 57.7 \tag{53}$$

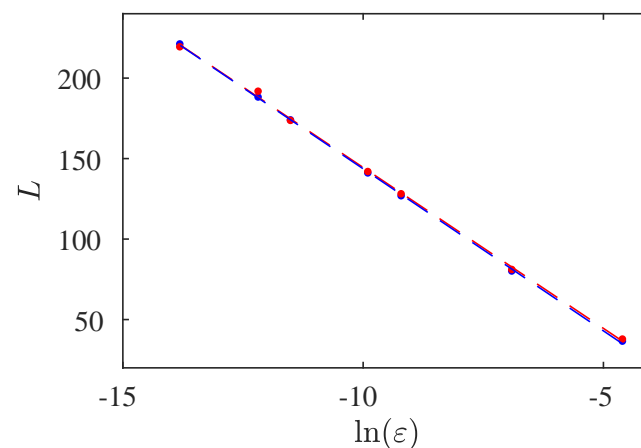Note that both equations verify the characteristic relation given by Equation (50) with $A \cong -1/c$.

Figure 12. Manneville map. Characteristic relation for $c = 0.05$. Blue points: density technique. Red points: numerical data. Blue dashed line: linear approximation for theoretical data, $A = -20.14$. Red dashed line: linear approximation for numerical data, $A = -19.99$.

The relation between the number of iterations in laminar and non-laminar phases, σ, can be calculated. Figure 13 shows this relation. We observe that σ has a linear variation with $\ln(\varepsilon)$. Remember that $\sigma = L/C$, where L has a linear dependence on $\ln(\varepsilon)$, and $L + C = constant$; therefore, C is also a linear function of $\ln(\varepsilon)$, which implies that σ is a linear function with $\ln(\varepsilon)$. σ increases as ε decreases, that is, the trajectory spends more time in the laminar zone for lower ε. From the figure, we note high accuracy between the numerical and theoretical results.
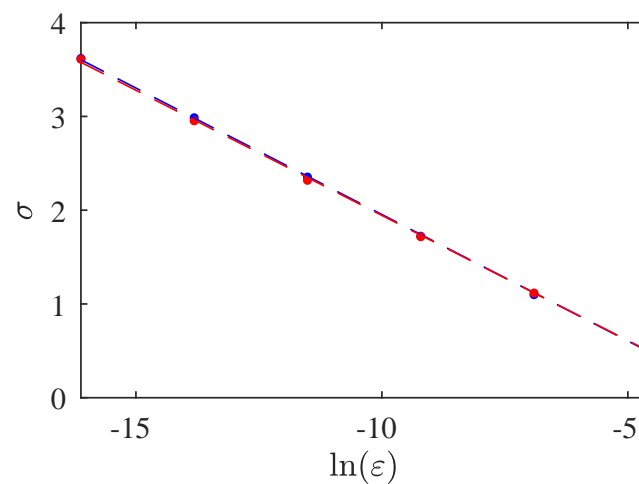
Figure 13. Manneville map. $\sigma(\varepsilon)$ for $c = 0.05$. Blue points: density technique. Red points: numerical data. Blue dashed line: linear interpolation of the theoretical results. Red dashed line: linear interpolation of the numerical data.

Finally, we calculate the number of crosses between the laminar and non-laminar phases by the total number of iterations for several values of the control parameter ε

$$\frac{N_{lc}}{N_t} = \frac{\sigma}{L(\sigma + 1)}, \tag{54}$$

Figure 14 shows the comparison between numerical and theoretical results. The red points and the red dashed line are the numerical data, blue points and the dashed blue line the theoretical ones. We observe good accuracy between them. As ε grows, so does N_{lc}. This behavior mainly occurs because the average laminar length, L, decreases for increasing ε.
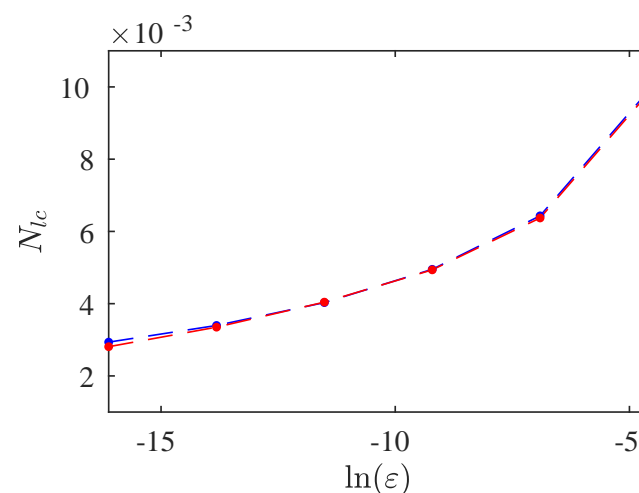

Figure 14. Manneville map. Number of crosses between the laminar and non-laminar phases for $c = 0.05$. Blue points and line: density technique. Red points and line: numerical data.

6. Conclusions

We presented a new methodology to evaluate the reinjection probability density, the probability density of the laminar lengths, the characteristic relation, the number of iterations in laminar and non-laminar phases, the intermittency factor, and the number of crosses between the laminar and non-laminar zones in chaotic intermittency. This methodology is obtained using the Perron–Frobenius operator to transform random variables, and we called it the density technique because it uses the invariant density of the maps. We

introduced and applied this technique to calculate the statistical properties in two maps, the cusp map (Equation (25)) and the classical Manneville map (Equation (41)). The cusp map given by Equation (25) has symmetry about the axis $x = 0$; however, the Manneville map has no symmetry. Accordingly, we applied the new methodology in symmetric and non-symmetric maps.

The classical studies about intermittency assume uniform RPD (see [1,2] and references therein). In the last few years, it has been found that the reinjection process is more complex, where uniform reinjection is only a case. This more complex process generates different characteristic relations that depend on the RPD function (see [3]). Therefore, an accurate evaluation of the RPD function is very important to calculate other statistical variables and to describe correctly the intermittency phenomenon. Recent research considers a less restrictive assumption of a constant density at points that govern the reinjection process, i.e., pre-reinjection points [3,30,40]. This assumption allows for obtaining exponential RPD functions (see Equation (34)).

The new methodology described in this paper does not introduce any assumption about the density at pre-reinjection points; it uses the invariant density of the map to calculate the RPD function and the other statistical properties (see Equations (15), (16), (18)–(24)). Additionally, Equations (15), (16), (18)–(24) determine explicitly the relationship between the statistical properties in chaotic intermittency and the map invariant density. Since the density technique does not introduce any hypothesis about density at pre-reinjection points, the new RPD functions are more accurate than those calculated with M function methodology and the classical theory (constant RPDs).

We carried out several comparisons of the theoretical results obtained by the density technique with those calculated by the M function methodology, by the classical theory of intermittency, and with numerical data. For all tests, the best results were obtained by the density technique. The results of the density technique are more accurate than those of the M function methodology and the classical theory. We emphasize that the RPD functions calculated with the density technique have broader behavior than the one expected by uniform reinjection, as can be seen in Equations (32) and (48) moving away from constant RPD.

To evaluate the convergence rate, we used two different error measures, E_r and D_r, given by Equation (39). For both studied maps, we have performed several tests with different values of the parameter ε, the length of laminar interval c, and the number of sub-intervals N_s. In all these tests, for the density technique, the error measures, D_r and E_r, decrease as the number of reinjected points increases, showing that the new theoretical evaluation approximates more accurately the random values of the numerical RPD as the number of reinjected points grows. We have calculated the rate of convergence of D_r and E_r, and we have found that the process is convergent with the rate of convergence $O(\frac{1}{N^p})$ with $0.4 \lesssim p \lesssim 0.5$. In addition, we emphasize that the density technique works better than classical theory and obtains RPDs with more accuracy than the M function methodology.

We have evaluated the characteristic relation, the number of iterations in laminar and non-laminar phases, the intermittency factor, and the number of crosses between the laminar and non-laminar phases (see Figures 12–14, and Tables 1 and 2). In all cases, we have found high accuracy between the new theoretical results and the numerical data. Additionally, the new methodology has shown accuracy for maps with and without symmetry. Therefore, the reinjection process is independent of the map symmetry.

To predict theoretical RPD functions, the density technique has the advantage that does not need to use numerical or experimental data. However, it has the drawback that we have to know the invariant density of the map. We can conclude that the density technique is a useful tool to calculate the statistical properties of the intermittency phenomenon.

Author Contributions: Conceptualization, S.E. and E.d.R.; methodology, S.E.; software, S.E.; validation, S.E., D.L.; formal analysis, S.E. and E.d.R.; investigation, S.E. and E.d.R.; resources, S.E., E.d.R. and D.L.; writing—original draft preparation, S.E.; writing—review and editing, S.E. and E.d.R.;

Abbreviations

The following abbreviations are used in this manuscript:

PDLL Probability density of the laminar lengths
RHS Right-hand side
RPD Reinjection probability density function

References

1. Schuster, H.; Just, W. *Deterministic Chaos*; Wiley VCH: Mörlenbach, Germany, 2005.
2. Nayfeh, A.; Balachandran, B. *Applied Nonlinear Dynamics*; Wiley: New York, NY, USA, 1995.
3. Elaskar, S.; del Rio, E. *New Advances on Chaotic Intermittency and Its Applications*; Springer: Cham, Switzerland, 2017.
4. Manneville, P. Intermittency, self-similarity and $1/f$ spectrum in dissipative dynamical systems. *J. Phys.* **1980**, *41*, 1235–1243. [CrossRef]
5. Dubois, M.; Rubio, M.; Berge, P. Experimental evidence of intermittencies associated with a subharmonic bifurcation. *Phys. Rev. Lett.* **1983**, *16*, 1446–1449. [CrossRef]
6. Stavrinides, S.; Miliou, A.; Laopoulos, T.; Anagnostopoulos, A. The intermittency route to chaos of an electronic digital oscillator. *Int. J. Bifurc. Chaos* **2008**, *18*, 1561–1566. [CrossRef]
7. Krause, G.; Elaskar, S.; del Rio, E. Type I intermittency with discontinuous reinjection probability density in a truncation model of the derivative nonlinear Schrödinger equation. *Nonlinear Dynam.* **2014**, *77*, 455–466. [CrossRef]
8. Sanchez-Arriaga, G.; Sanmartin, J.; Elaskar, S. Damping models in the truncated derivative nonlinear Schrödinger equation. *Phys. Plasmas* **2007**, *14*, 082108. [CrossRef]
9. Nishiura, Y.; Ueyama, D.; Yanagita, T. Chaotic pulses for discrete reaction diffusion systems. *SIAM J. App. Dyn. Syst.* **2005**, *4*, 723–754. [CrossRef]
10. De Anna, P.; Le Borgne, T.; Dentz, M.; Tartakovsky, A.; Bolster, D.; Davy, P. Flow intermittency, dispersion and correlated continuous time random walks in porous media. *Phys. Rev. Lett.* **2013**, *110*, 184502. [CrossRef] [PubMed]
11. Stan, C.; Cristescu, C.; Dimitriu, D. Analysis of the intermittency behavior in a low-temperature discharge plasma by recurrence plot quantification. *Phys. Plasmas* **2010**, *17*, 042115. [CrossRef]
12. Chian, A. *Complex System Approach to Economic Dynamics. Lecture Notes in Economics and Mathematical Systems*; Springer: Berlin, Germany, 2007.
13. Zebrowski, J.; Baranowski, R. Type I intermittency in nonstationary systems: Models and human heart-rate variability. *Physica A* **2004**, *336*, 74–86. [CrossRef]
14. Paradisi, P.; Allegrini, P.; Gemignani, A.; Laurino, M.; Menicucci, D.; Piarulli, A. Scaling and intermittency of brains events as a manifestation of consciousness. *AIP Conf. Proc.* **2012**, *1510*, 151–161.
15. Fujisaka, H; Kamifukumito, H.; Inoue, M. Intermittency associated with the breakdown of the chaos symmetry. *Prog. Theor. Phys.* **1983**, *69*, 333–337. [CrossRef]
16. Hnatič, M.; Honkonen, J.; Lučivjanský, T. Symmetry breaking in stochastic dynamics and turbulence. *Symmetry* **2019**, *11*, 1193. [CrossRef]
17. Manneville, P.; Pomeau, Y. Intermittency and the Lorenz model. *Phys. Lett.* **1979**, *75A*, 1–2. [CrossRef]
18. Pomeau, Y.; Manneville, P. Intermittent transition to turbulence in dissipative dynamical systems. *Commun. Math. Phys.* **1980**, *74*, 189–197. [CrossRef]
19. Price, T.; Mullin, P. An experimental observation of a new type of intermittency. *Physica D* **1991**, *48*, 29–52. [CrossRef]
20. Platt, N.; Spiegel, E.; Tresser, C. On-off intermittency: A mechanism for bursting. *Phys. Rev. Lett.* **1993**, *70*, 279–282. [CrossRef]

21. Pikovsky, A.; Osipov, G.; Rosenblum, M.; Zaks, M.; Kurths, J. Attractor–repeller collision and eyelet intermittency at the transition to phase synchronization. *Phys. Rev. Lett.* **1997**, *79*, 47–50. [CrossRef]
22. Lee, K.; Kwak, Y.; Lim, T. Phase jumps near a phase synchronization transition in systems of two coupled chaotic oscillators. *Phys. Rev. Lett.* **1998**, *81*, 321–324. [CrossRef]
23. Hramov, A.; Koronovskii, A.; Kurovskaya, M.; Boccaletti, S. Ring intermittency in coupled chaotic oscillators at the boundary of phase synchronization. *Phys. Rev. Lett.* **2006**, *97*, 114101. [CrossRef]
24. Del Rio, E.; Elaskar, S. Type III intermittency without characteristic relation. *Chaos* **2021**, *31*, 043127. [CrossRef]
25. Hirsch, J.; Huberman, B.; Scalapino, D. Theory of intermittency. *Phys. Rev. A* **1982**, *25*, 519–532. [CrossRef]
26. Elaskar, S.; del Rio, E.; Donoso, J. Reinjection probability density in type III intermittency. *Phys. A* **2011**, *390*, 2759–2768. [CrossRef]
27. Del Rio, E.; Sanjuan, M.; Elaskar, S. Effect of noise on the reinjection probability density in intermittency. *Commun. Nonlinear Sci. Numer. Simulat.* **2012**, *17*, 3587–3596. [CrossRef]
28. Del Rio, E.; Elaskar, S.; Makarov, S. Theory of intermittency applied to classical pathological cases. *Chaos* **2013**, *23*, 033112. [CrossRef] [PubMed]
29. del Rio, E.; Elaskar, S.; Donoso, J. Laminar length and characteristic relation in type I intermittency. *Commun. Nonlinear Sci. Numer. Simulat.* **2014**, *19*, 967–976. [CrossRef]
30. del Río, E.; Elaskar S.: On the intermittency theory. *Int. J. Bifurc. Chaos* **2016**, *26*, 1650228. [CrossRef]
31. Elaskar, S.; del Río, E.; Costa, A. Reinjection probability density for type III intermittency with noise and lower boundary of reinjection. *J. Comp. Nonlinear Dynam.* **2017**, *12*, 031020-11. [CrossRef]
32. Elaskar, S.; del Río, E.; Gutierrez Marcantoni, L. Non-uniform reinjection probability density function in type V intermittency. *Nonlinear Dynam.* **2018**, *92*, 683–697. [CrossRef]
33. del Rio, E.; Elaskar S. Experimental evidence of power law reinjection in chaotic intermittency. *Commun. Nonlinear Sci. Numer. Simulat.* **2018**, *64*, 122–134.
34. Elaskar, S.; del Rio, E. Discontinuous reinjection probability density function in type v intermittency. *J. Comp. Nonlinear Dynam.* **2018**, *13*, 121001. [CrossRef]
35. del Rio, E.; Elaskar, S. Experimental results versus computer simulations of noisy Poincare maps in an intermittency scenario. *Regul. Chaotic Dyn.* **2020**, *25*, 281–294. [CrossRef]
36. Hemmer, P. The exact invariant density for a cusp-shaped return map. *J. Phys. A Math. Gen.* **1984**, *17*, L247–L249. [CrossRef]
37. Beck, C.; Schogl, F. *Thermodynamics of Chaotic Systems*; Cambridge University Press: Cambridge, UK, 1993.
38. Del Rio, E.; Elaskar, S. New characteristic relation in type II intermittency. *Int. J. Bifurc. Chaos* **2010**, *20*, 1185–1191. [CrossRef]
39. Lasota, A.; Mackey, M. *Probabilistic Properties of Deterministic Systems*; Cambridge University Press: Cambridge, UK, 1985.
40. Elaskar S.; del Rio E.; Zapico, E. Evaluation of the statistical properties for type-II intermittency using the Perron-Frobenius operator. *Nonlinear Dynam.* **2016**, *86*, 1107–1116. [CrossRef]
41. Burden, R.; Faires, J.; Burden, A. *Numerical Analysis*, 10th ed.; Cengage Learning: Boston, MA, USA, 2014.
42. Thaler, M. The invariant densities for maps modeling intermittency. *J. Stat. Phys.* **1994**, *79*, 739–741. [CrossRef]